APL Materials

Cerium-based RCo_5 (R = Ce, $La_{0.35}Ce_{0.65}$, and misch-metal) type nanocrystalline hard magnetic materials with high coercivity

Cite as: APL Mater. **7**, 091108 (2019); https://doi.org/10.1063/1.5104295
Submitted: 26 April 2019 . Accepted: 02 September 2019 . Published Online: 18 September 2019

Wen-Liang Zuo, Jeotikanta Mohapatra, J. Ping Liu, Tong-Yun Zhao, Feng-Xia Hu, Ji-Rong Sun, Yong-Feng Li, Xue-Feng Zhang, and Bao-Gen Shen

Cerium-based RCo_5 (R = Ce, $La_{0.35}Ce_{0.65}$, and misch-metal) type nanocrystalline hard magnetic materials with high coercivity

Cite as: APL Mater. 7, 091108 (2019); doi: 10.1063/1.5104295
Submitted: 26 April 2019 • Accepted: 2 September 2019 •
Published Online: 18 September 2019

Wen-Liang Zuo,[1,2,3,a)] Jeotikanta Mohapatra,[2,a)] J. Ping Liu,[2,b)] Tong-Yun Zhao,[3] Feng-Xia Hu,[3] Ji-Rong Sun,[3] Yong-Feng Li,[4] Xue-Feng Zhang,[4] and Bao-Gen Shen[3,b)]

AFFILIATIONS

[1]School of Sciences, MOE Key Laboratory for Nonequilibrium Synthesis and Modulation of Condensed Matter, Xi'an Jiaotong University, Xi'an, Shaanxi 710049, China
[2]Department of Physics, The University of Texas at Arlington, Arlington, Texas 76019, USA
[3]State Key Laboratory of Magnetism, Institute of Physics, Chinese Academy of Sciences, Beijing 100190, People's Republic of China
[4]School of Sciences, Inner Mongolia University of Science and Technology, Baotou 014010, People's Republic of China

[a)]**Contributions:** W.-L. Zuo and J. Mohapatra contributed equally to this work.
[b)]**Authors to whom correspondence should be addressed:** pliu@uta.edu and shenbg@aphy.iphy.ac.cn

ABSTRACT

Nanocrystalline RCo_5 (R = Ce, $La_{0.35}Ce_{0.65}$, and misch-metal noted as MM) ribbons with hexagonal crystal structure and an average grain size of 5 nm have been prepared via a one-step melt-spinning technique. Coercivity as high as 13.0, 13.8, and 10.9 kOe has been obtained at 300 K for the $CeCo_5$, $La_{0.35}Ce_{0.65}Co_5$, and $MMCo_5$ ribbons, respectively. High thermal stability is also achieved as shown by the high coercivity of 9.3 kOe, 10.2 kOe, and 8.8 kOe at 400 K for $CeCo_5$, $La_{0.35}Ce_{0.65}Co_5$, and $MMCo_5$ ribbons, respectively. The coercivity mechanism is studied by magnetization analysis and microstructural observations. The nanocrystalline grains promote a strong exchange interaction, as indicated by the positive δM and the relatively high remanence ratio (~0.8). In addition, the temperature dependence of coercivity of RCo_5 ribbons shows the low coercivity temperature coefficient of −0.2% to −0.25%/K.

I. INTRODUCTION

Among various rare-earth transition-metal intermetallic compounds, RCo_5 (R = rare-earth elements) compounds are particularly interesting due to their extremely high magnetocrystalline anisotropy and very high Curie temperature.[1,2] The $SmCo_5$ compound has the highest uniaxial magnetocrystalline anisotropy (20×10^7 erg/cm^3) and is the major phase of the first generation of rare-earth permanent magnets.[2] In comparison to $SmCo_5$, the other RCo_5 compounds possess similar inherent magnetic properties, however they have not been used as permanent magnets because of technical difficulties in achieving proper microstructures necessary for developing high coercivity. For instance, even though $CeCo_5$ exhibits quite high magnetocrystalline anisotropy (7.2×10^7 erg/cm^3),[1,3,4] the reported magnetic coercivity reaches only 3%–5% of the corresponding anisotropy field (H_k).[2,5]

Recent research for the new economical alternatives to the current commercial rare-earth permanent magnets showed that despite having the mixed Ce^{3+}/Ce^{4+} valency problem,[6] typically adverse for the magnetocrystalline anisotropy, the Ce-substituted $Nd_2Fe_{14}B$ magnet systems are comparable with the commercial high-flux grade magnets and also have lower material cost.[6,7] Attempts have also been made to replace Sm by Ce or La, or other low cost mixed rare-earths like MM (25–35 wt. % La, 45–55 wt. % Ce, 4–10 wt. % Pr, 14–18 wt. % Nd) in $SmCo_5$-type magnets.[8,9] Unfortunately, the coercivity of the prepared RCo_5 hard magnetic materials is low.[2,5,9]

An alternative magnet is the $Sm_2Fe_{17}N_3$ phase due to its high saturation magnetization (1.54–1.57 T), anisotropy field (21–26 T), and Curie temperature (~470 °C).[10] More importantly, the $Sm_2Fe_{17}N_3$ phase has been obtained in powder form by the nitrogenation of Sm_2Fe_{17} alloy powder. However, the conventional sintering techniques cannot be applied to the production of magnets because the $Sm_2Fe_{17}N_3$ phase lacks stability at high temperatures and decomposes into α-Fe and SmN. It is therefore essential to develop new magnetic materials for more applications in modern products which require strong permanent magnets. In this study, we have prepared nanocrystalline RCo_5 (R = Ce, $La_{0.35}Ce_{0.65}$, MM) ribbons with hexagonal phase and an average grain size of 5 nm via a one-step melt-spinning technique. The average nanocrystal size is calculated by using a statistical analysis of 70–100 nanocrystals. Magnetic properties of the ribbons are investigated systematically, and the results show high promise for the Ce-based RCo_5 magnets for future applications with high performance and low cost.

II. MATERIALS AND METHODS

RCo_5 (R = Ce, $La_{0.35}Ce_{0.65}$, MM) ingots were prepared by arc-melting in a high purity argon gas atmosphere. The purity of starting materials is 99% for Ce and $La_{0.35}Ce_{0.65}$ and MM = 28.27 wt. % for La, 50.46 wt. % for Ce, 5.22 wt. % for Pr, 15.66 wt. % for Nd, ≤ 1 wt. % for others, and 99.95% for Co. The ingots were melted five times to ensure homogeneity, and then a part of the ingot was ground down into powders of less than 150 μm in particle size. The phase structure was determined by X-ray powder diffraction (XRD) with Cu Kα radiation. The RCo_5 ribbons were prepared by induction melting the ingot in a quartz tube with a nozzle size of 0.1 mm and then ejected onto the surface of a water-cooled copper wheel with a surface velocity of 40–60 m/s. The grain size of the RCo_5 ribbons was determined by transmission electron microscopy (TEM). Magnetic properties were measured by a DynaCool physical property measurement system (PPMS) with a maximum field of 90 kOe and in the temperature range of 5–500 K.

III. RESULTS AND DISCUSSION

The art of making high coercivity magnetic materials is to control the microstructure at the nanoscale.[11,12] The H_C value will increase with decreasing grain size until it reaches the level of the ferromagnetic domain wall width.[11] Thus, to reduce the grain size is of paramount importance for obtaining high performance in hard magnetic materials. Rapid quenching via melt-spinning is an effective way to prepare ultra-small-grain materials. However, the grain size of RCo_5 ribbons prepared via the regular melt-spinning technique is in the range of 50–100 nm.[13] In order to refine the grain size down to few nanometers, the melt-spinning speed is increased to 50 m/s.[14] Because the speed 50 m/s is almost the limitation of the melt-spinning facility we used, we have reduced the nozzle size of the quartz tube from the traditional size (~0.5 to 1 mm) to 0.1 mm, which resulted in a faster cooling rate and much smaller grains. Figures 1(a) and 1(b) show the XRD patterns for RCo_5 (R = Ce, $La_{0.35}Ce_{0.65}$, MM) ingots and ribbons, respectively. Both the ingots and ribbons primarily have the hexagonal RCo_5 phase crystalline structure with space group of P6/mnm. The XRD patterns of $CeCo_5$ ingots show minor impurity. However, these impurity peaks are absent in the XRD pattern of the ribbons, which could be due to the fast cooling process that impeded the formation of impurity phases.[15] In addition, all the ribbons give broader diffraction peaks, which is expected and is attributed to the grain refinement.[5,15] Transmission electron microscopy (TEM) was performed in order to investigate the grain size and the uniformity of the as-prepared RCo_5 ribbons. The TEM image and the corresponding nanocrystal size distribution histogram [shown in Figs. 2(a) and 2(b), respectively] demonstrate that the $CeCo_5$ ribbons consist of nanocrystalline grains of average size around 5 nm. Figure 2(c) shows the selected area diffraction (SAED) pattern of $CeCo_5$ ribbons. The SAED pattern indicates a set of rings corresponding to the reflection from the crystal planes of the $CeCo_5$ phase. The detailed structure of the ribbons is further analyzed using the HRTEM image. Figure 2(d) depicts that the $CeCo_5$ nanocrystals (yellow dotted ovals) are well separated by the amorphous Ce–Co matrix. Figures 2(e) and 2(f) and Figs. 2(g) and 2(h) show the Fast Fourier transform (FFT) patterns and the corresponding inverse Fast Fourier transform (IFFT) patterns of the two selected areas of the HRTEM micrograph as indicated by the red arrows, respectively. The FFT pattern of the crystalline region shows hexagonal symmetry, and the distance between the lattice fringe is found to be 0.211 nm, which is close to the (200) planes of the $CeCo_5$. The FFT and IFFT of the grain boundary confirm that the $CeCo_5$ nanocrystals are well separated by the amorphous phase. Thus, the ultrafine grains can result in a high coercivity based on the

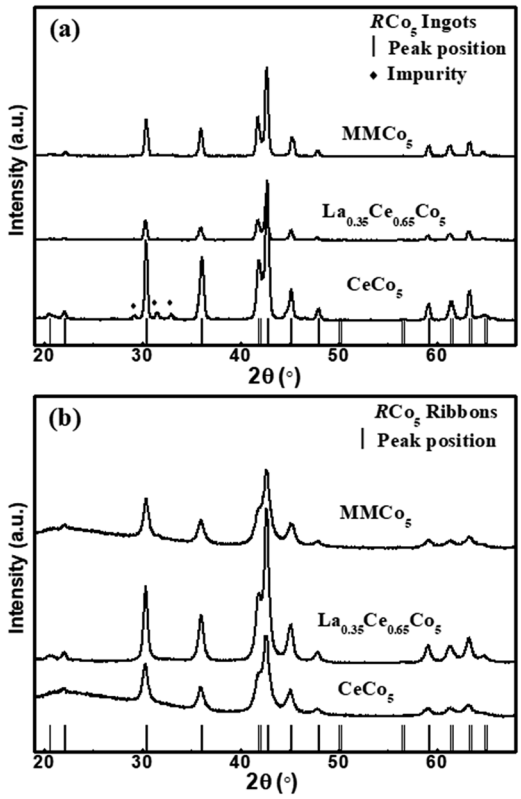

FIG. 1. The XRD pattern of RCo_5 (R = Ce, $La_{0.35}Ce_{0.65}$, MM): (a) ingots and (b) ribbons.

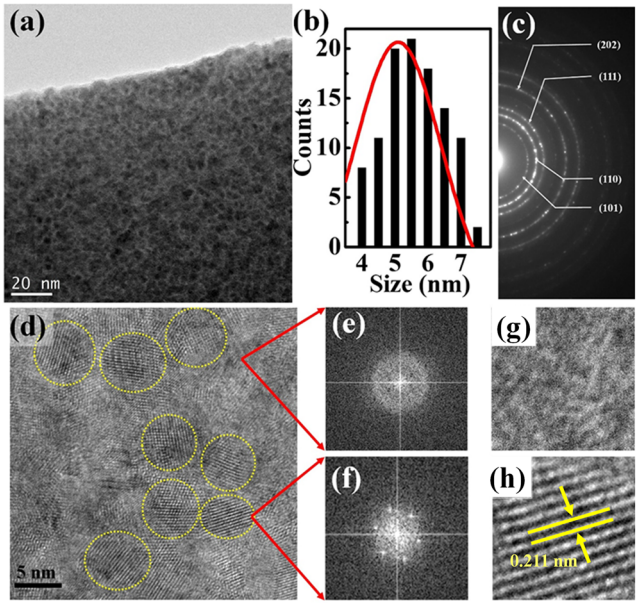

FIG. 2. (a) TEM micrograph and (b) the corresponding nanocrystal size distribution histograms of $CeCo_5$ ribbons. (c) Selected area electron diffraction (SAED) pattern of $CeCo_5$ ribbons. (d) HRTEM image of $CeCo_5$ ribbon showing the nanocrystals are well separated by Ce-Co amorphous phase. [(e) and (f)] Fast Fourier transforms (FFTs) and (g) and (h) inverse fast Fourier transforms (IFFTs) of selected regions of the HRTEM image.

coherent rotation of the magnetization which has been observed in the prepared RCo_5 ribbons.

Figure 3(a) shows the temperature dependence magnetization loops of the $CeCo_5$ ribbons. The saturation magnetization (M_S) of 62 emu/g and coercivity (H_C) of 13 kOe at 300 K are obtained in the $CeCo_5$ ribbons. It is worthwhile to mention that the achieved H_C value is 1.5–2 times higher than that of the $CeCo_5$ prepared by traditional methods.[2,5,16] The high coercivity in the $CeCo_5$ ribbons can be ascribed to the existence of noncoupled $CeCo_5$ nanocrystals, which is caused by the amorphous Ce–Co phase formed at the grain boundaries.[17] In order to understand the coercivity mechanism, the temperature dependence of H_C and the dependence of δM on the reverse field (Henkel plot) are investigated. According to the magnetic hardening mechanism by Kronmüller *et al.*, the intrinsic coercivity strongly depends on the microstructure of the magnet, which can be phenomenologically expressed by the following equation:[18,19]

$$\mu_0 H_c = \alpha_k \alpha_{ex} \frac{K_1 \mu_0}{M_s} - N_{eff} M_s,$$

where K_1, N_{eff}, and M_S are the first-order magnetic anisotropy constant, the magnetostatic interaction parameter, and the saturation magnetization, respectively. The coefficient α_k reflects the local reduction of crystal anisotropy of inhomogeneous surface regions and generally incorporates the effect of the sample microstructure. The α_{ex} describes the adverse effect of exchange coupling between neighboring grains on the coercivity. The microstructural parameter $\alpha_k \alpha_{ex}$ has not been analyzed separately in nanocrystalline alloys, but several researchers have shown that the $\alpha_k \alpha_{ex} \geq 0.80$ for a nonexchange coupled magnet with nearly perfect grain surface.[20] However, it decreases with an increase in the intergranular exchange coupling.[19] These parameters can be determined by linear fitting $\frac{\mu_0 H_c}{M_s}$ against $\frac{K_1 \mu_0}{M_s^2}$ [See Fig. 3(b)]. The temperature dependent values of K_1 and M_S are taken from the previous work on the $CeCo_5$ single crystal.[3] The values of $\alpha_k \alpha_{ex}$ and N_{eff} are obtained by using a linear fit, and they are 0.24 and 0.19, respectively. As expected for nanocrystalline melt-spun alloy ribbons, the microstructural

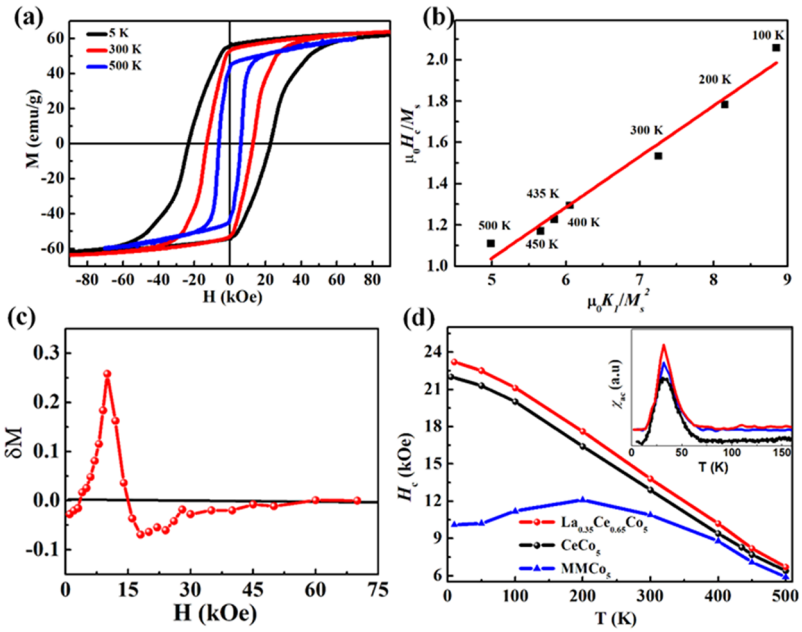

FIG. 3. (a) The hysteresis loops of $CeCo_5$ ribbons at the temperature of 5 K, 300 K, and 500 K, respectively. (b) $\mu_0 H_c / M_s$ against $2K_1\mu_0/M_s^2$ on different temperatures for $CeCo_5$ ribbons. (c) The δM-H plots of the nanocrystalline $CeCo_5$ ribbons. (d) The temperature dependence of coercivity for $CeCo_5$, $La_{0.35}Ce_{0.65}Co_5$, and $MMCo_5$ ribbons. The corresponding inset shows the temperature dependence of ac susceptibility χ_{ac}.

parameters obtained are somewhat smaller values, which is mainly due to the refined grain size. The uniform nanocrystalline grains lead to enhanced exchange interaction and consequently decrease the local stray fields. In fact, for the noninteracting nanocrystalline systems, the remanence ratio, $M_R/Ms = 0.5$. However, in our case, the M_R/Ms ratio is 0.8, which indicates the exchange coupling between the nanograins and amorphous Fe–Co alloys within the $CeCo_5$ ribbons. It is worth mentioning that the coercivity mechanism of the nanocrystalline exchange-coupled magnets cannot be completely determined by the above approach because of intergranular interactions among the fine grains. Furthermore, since the average grain size of the prepared $CeCo_5$ ribbons is 5 nm, smaller than a typical domain size, therefore, both "nucleation" and "pinning" mechanisms are not applicable. Although a direct measurement is not possible under the current condition, it is likely that the coercivity is resulted from the magnetization reversal as single domain structure in isolated magnetic nanocrystals. On the other hand, we realized that mechanisms of coercivity in nanostructured ferromagnetic materials are not well understood yet. Some related phenomena like interaction domains cannot be directly characterized in a quantitative way. It is therefore necessary to carry more investigations on this topic in the future.

To further confirm the exchange interactions between the $CeCo_5$ nanograins, Henkel plots (δM-H) were measured. The expression for δM is defined as $\delta M = M_d(H) - (1 - 2M_R(H))$,[11,19,24] where M_d is the reduced initial demagnetization remanence and M_R is the reduced initial remanence. The δM curve with a positive peak indicates magnetic exchange coupling between the grains which supports the magnetized state, whereas a negative peak indicates magnetostatic interactions that tend to demagnetize the system. In our case, the δM value for $CeCo_5$ ribbons [Fig. 3(c)] is initially positive and reached 0.3 when the reversal field increased to 10 kOe. With a further increase of the reversal field, the δM becomes slightly negative due to the dominating contributions from the magnetostatic interactions. The positive δM value indicates the existence of the exchange type of interaction among the grains. Moreover, for the prepared $CeCo_5$ ribbons, the average grain size is around 5 nm, which is larger than the domain wall width $\pi\sqrt{A/K_1} \approx 3.7$ nm. As in our case, the average grain size is slightly larger than the domain wall width and the exchange coupling impedes the magnetization to follow the local anisotropy axis and hence results in a high M_R/Ms ratio.[12,21] It should be mentioned that the high M_R/M_S ratio could also result from the strong exchange interaction between the $CoCo_5$ grains and amorphous boundary like the hard/soft exchanged coupling magnets. Moreover, the amorphous Ce–Co phase possesses an M_S value comparable to that of $CeCo_5$ phase;[22] hence, the exchanged coupling could be beneficial for high remanence.

The temperature dependent coercivity analysis for $CeCo_5$ and $La_{0.35}Ce_{0.65}Co_5$ ribbons shows a linear increase in coercivity with the decrease in temperature from 500 K to 50 K [see in Fig. 3(d)]. However, the coercivity values for $MMCo_5$ ribbons show a completely different temperature dependence as compared to that of Ce-based RCo_5 ribbons. Especially, when the temperature is lower than 200 K, the coercivity values even show a slight drop, which is mainly due to the easy-plane anisotropy of $NdCo_5$ constituent.[3] The corresponding temperature coefficient of coercivity is calculated by the following formula:[23,24]

$$\beta = \frac{H_c(T) - H_c(T_0)}{H_c(T_0)(T - T_0)} * 100\%. \quad (1)$$

The calculated result shows that the β for $CeCo_5$, $La_{0.35}Ce_{0.65}Co_5$, and $MMCo_5$ ribbons are ~−0.25%, −0.26%, and −0.2%/K between 300 K and 500 K, which are lower than that of the commercial Nd–Fe–B sintered magnets (−0.6%/K) and the high-coercivity hot-deformed Nd–Fe–B permanent magnets (−0.45%/K).[24] At a high temperature (450 K), the coercivity of RCo_5 ribbons exceed 7 kOe (Table I), which is close to the coercivity of 8% Dy containing Nd–Fe–B magnets (NMX-36).[24] Especially, the coercivity shows a point of deviation from the linear increase at 5 K. Unfortunately, the low temperature behavior has not been studied in detail, and most of the reports about the magnetocrystalline anisotropy field of $CeCo_5$ are larger than 77 K.[3] In order to explore this phenomenon, we measured the temperature dependence of ac susceptibility χ_{ac} of RCo_5 ribbons from 5 K to 160 K with ac amplitude 5 Oe and frequency 4997 Hz, which is shown in the inset of Fig. 3(d). It can be seen that a broad peak appears at the temperature of 32 K. It is known that the position of the peak of χ_{ac} represents the weakest magnetocrystalline anisotropy at that temperature. Thus, it is often used for detection of the change temperature of easy-magnetization direction (also called spin reorientation). Thus, the deviation of H_C from the linear trend at 5 K is mainly due to the changes of magnetocrystalline anisotropy field from spin reorientation. Meanwhile, it demonstrates that the spin reorientation temperature (T_s) of $CeCo_5$ and $La_{0.35}Ce_{0.65}Co_5$ is about 32 K, which is lower than that of Nd–Fe–B and hence beneficial for the low temperature applications. The high coercivity, low coercivity temperature coefficient, and low T_s of the prepared Ce-based RCo_5 ribbons imply a great potential of the application for abundant rare-earth based permanent magnets. Although the prepared RCo_5 ribbons showed a larger coercivity compared to the traditional preparing methods, the H_C value is still smaller than 20% of the corresponding anisotropy field (H_k). A precise control of nanocrystals size and shape can be utilized to improve the coercivity further.

TABLE I. The magnetic properties and grain size of RCo_5 ribbons.

	H_c (kOe) at different T (K)								
Samples	450	400	300	200	100	50	10	T_s (K)	Average grain size (nm)
$CeCo_5$	7.7	9.3	13.0	16.4	19.8	21.2	21.9	32	~5
$La_{0.35}Ce_{0.65}Co_5$	8.2	10.2	13.8	17.6	21.2	22.5	23.2	32	~5
$MMCo_5$	7.1	8.8	10.9	12.1	11.2	10.2	10.1	32	~5

IV. CONCLUSION

The ultrafine granular RCo_5 (R = Ce, $La_{0.35}Ce_{0.65}$, MM) ribbons with high coercivity have been prepared by one-step melt-spinning technology. The strong exchange-interaction among the nanograins of 5 nm in average size leads to the enhanced M_R/Ms ratio. The room temperature coercivity of $CeCo_5$ and $La_{0.35}Ce_{0.65}Co_5$ is 1.5–2 times higher than that of these magnets prepared by the traditional methods. More importantly, the coercivity values exceeding 7 kOe at the temperature 450 K and coercivity temperature coefficients of −0.2% to −0.25%/K are achieved, which are comparable or superior to the 8% Dy containing Nd–Fe–B magnets. The high coercivity and low coercivity temperature coefficients imply the great potential for developing the abundant rare-earth based permanent magnets.

ACKNOWLEDGMENTS

This work was supported by the National Basic Research Program of China (Grant No. 2014CB643702), the National Key Research and Development Program of China (Grant No. 2016YFB0700903), the National Natural Science Foundation of China (Grant Nos. 51590880, 51401235, and 51327806), the Knowledge Innovation Project of the Chinese Academy of Sciences (No. KJZD-EW-M05), the China Postdoctoral Science Foundation funded project (Grant No. 2017M623147), the Fundamental Research Funds for the Central Universities, the Word-Class Universities (Disciplines), and the Characteristic Development Guidance Funds for the Central Universities.

REFERENCES

[1] K. Strnat, G. Hoffer, J. Olson, W. Ostertag, and J. J. Becker, J. Appl. Phys. **38**(3), 1001 (1967).
[2] Y. Tawara and H. Senno, Jpn. J. Appl. Phys. **7**(8), 966 (1968).
[3] H. P. Klein and A. Menth, AIP Conf. Proc. **18**(1), 1177 (1974).
[4] M. T. Onyszczak, T. N. Lamichhane, S. L. Bud'ko, P. C. Canfield, and A. Palasyuk, J. Magn. Magn. Mater. **482**, 192 (2019); M. I. Bartashevich, T. Goto, R. J. Radwanski, and A. V. Korolyov, J. Magn. Magn. Mater. **131**(1), 61 (1994).
[5] E. A. Nesbitt, G. Y. Chin, P. K. Gallagher, R. C. Sherwood, and J. H. Wernick, J. Appl. Phys. **42**(4), 1530 (1971).
[6] A. K. Pathak, M. Khan, K. A. Gschneidner, Jr., R. W. McCallum, L. Zhou, K. Sun, K. W. Dennis, C. Zhou, F. E. Pinkerton, M. J. Kramer, and V. K. Pecharsky, Adv. Mater. **27**(16), 2663 (2015).
[7] J. M. D. Coey, Scr. Mater. **67**(6), 524 (2012).
[8] R. K. Chouhan and D. Paudyal, J. Alloys Compd. **723**, 208 (2017).
[9] S. Takata, Trans. Jpn. Inst. Met. **14**(6), 477 (1973).
[10] C. Lu, X. Hong, X. Bao, X. Gao, and J. Zhu, J. Alloys Compd. **784**, 980 (2019).
[11] A. S. Bolyachkin and S. V. Komogortsev, Scr. Mater. **152**, 55 (2018).
[12] G. Herzer, IEEE Trans. Magn. **26**(5), 1397 (1990).
[13] A. A. Kundig, R. Gopalan, T. Ohkubo, and K. Hono, Scr. Mater. **54**(12), 2047 (2006).
[14] L. Li, Z. Gao, Y. Ge, A. Yan, W. Zhang, and Y. Peng, J. Alloys Compd. **714**, 194 (2017).
[15] W.-L. Zuo, S.-L. Zuo, R. Li, T.-Y. Zhao, F.-X. Hu, J.-R. Sun, X.-F. Zhang, J. Ping Liu, and B.-G. Shen, J. Alloys Compd. **695**, 1786 (2017).
[16] J. J. Zhang, H. M. Gao, Y. Yan, X. Bai, F. Su, W. Q. Wang, and X. B. Du, J. Magn. Magn. Mater. **324**(20), 3272 (2012); W. Sun, K.-K. Song, M.-G. Zhu, Y.-K. Fang, N.-J. Yu, S. Wang, and W. Li, J. Supercond. Novel Magn. **31**(6), 1761 (2018); R.-M. Liu, D.-M. Zhu, L.-Y. Jia, C. Dan, J. Xiong, H. Guo-hui, Q. Wang, and L. Bing-shan, Ferroelectrics **522**(1), 122 (2018).
[17] J. Arcas, A. Hernando, C. Gómez-Polo, F. J. Castaño, M. Vázquez, A. Neuweiler, and H. Krönmuller, J. Phys.: Condens. Matter **12**(14), 3255 (2000).
[18] H. Kronmüller, K. D. Durst, and M. Sagawa, J. Magn. Magn. Mater. **74**(3), 291 (1988); A. Singh, V. Neu, S. Fähler, K. Nenkov, L. Schultz, and B. Holzapfel, Phys. Rev. B **77**(10), 104443 (2008); J. Fidler and T. Schrefl, J. Appl. Phys. **79**(8), 5029 (1996); C.-B. Rong, H.-W. Zhang, B.-G. Shen, and J. Ping Liu, Appl. Phys. Lett. **88**(4), 042504 (2006).
[19] X. C. Kou, H. Kronmüller, D. Givord, and M. F. Rossignol, Phys. Rev. B **50**(6), 3849 (1994); H.-W. Zhang, C.-B. Rong, J. Zhang, S.-Y. Zhang, and B.-G. Shen, Phys. Rev. B **66**(18), 184436 (2002); D. Goll and H. Kronmüller, Naturwissenschaften **87**(10), 423 (2000).
[20] J. Bauer, M. Seeger, and H. Kronmüller, J. Magn. Magn. Mater. **139**(3), 323 (1995); Z. W. Liu and H. A. Davies, J. Phys. D: Appl. Phys. **42**(14), 145006 (2009).
[21] G. Herzer, Scr. Metall. Mater. **33**(10), 1741 (1995).
[22] D. Malterre, J. Durand, A. Siari, and G. Marchal, J. Phys. Colloq. **49**(C8), C8 (1988).
[23] J. Liu, H. Sepehri-Amin, T. Ohkubo, K. Hioki, A. Hattori, T. Schrefl, and K. Hono, Acta Mater. **82**, 336 (2015); R. Li, R. X. Shang, J. F. Xiong, D. Liu, H. Kuang, W. L. Zuo, T. Y. Zhao, J. R. Sun, and B. G. Shen, AIP Adv. **7**(5), 056207 (2017).
[24] T. Akiya, J. Liu, H. Sepehri-Amin, T. Ohkubo, K. Hioki, A. Hattori, and K. Hono, Scr. Mater. **81**, 48 (2014).